ACS SENSORS

pubs.acs.org/acssensors
Article

Colorimetric CRISPR Biosensor: A Case Study with Salmonella Typhi

Ana Pascual-Garrigos, Beatriz Lozano-Torres, Akashaditya Das, and Jennifer C. Molloy*

Cite This: ACS Sens. 2025, 10, 717−724
Read Online

ABSTRACT: There is a critical need to implement a sensitive and specific point-of-care (POC) biosensor that addresses the instrument limitations and manufacturing challenges faced in resource-constrained contexts. In this paper we focus on enteric fever which is a highly contagious and prevalent infection in low- and middle-income countries. Although easily treatable, its ambiguous symptoms paired with a lack of fast, accurate and affordable diagnostics lead to incorrect treatments which exacerbate the disease burden, including increasing antibiotic resistance. In this study, we develop a readout module for CRISPR-Cas12a that produces a colorimetric output that is visible to the naked eye and can act as a cascade signal amplifier in any CRISPR assay based on trans-cleavage. We achieve this by immobilizing an oligo covalently linked to a β-galactosidase (LacZ) enzyme, which is cleaved in the presence of DNA target-activated CRISPR-Cas12a. Upon cleavage, the colorimetric enzyme is released, and the supernatant transferred to an environment containing X-Gal producing an intense blue color. This method is capable of detecting amplified bacterial genomic DNA and has a lower limit of detection (LoD) to standard fluorescent assays while removing the requirement for costly equipment. Furthermore, it remained active 4 weeks after lyophilization, allowing for the possibility of shipment without cold chain, significantly reducing deployment costs.

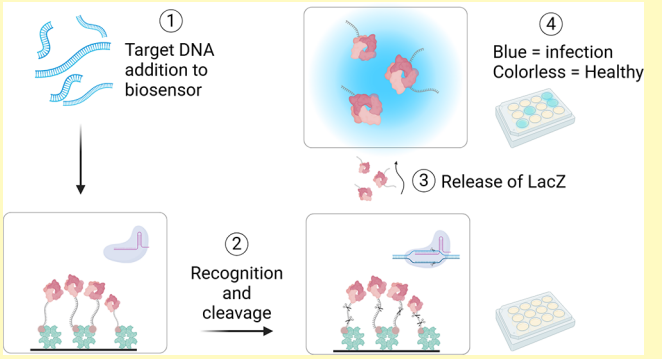

KEYWORDS: *CRISPR-Cas12a, colorimetric, β-galactosidase, DNA, biosensor*

Enteric fever is a highly contagious infection caused by *Salmonella enterica* serovar Typhi (*S.* Typhi) and Paratyphi A, B & C (*S.* Paratyphi).[1] In the past decade, it is estimated that there are 9−17.8 million cases of the disease and around 100,000−208,000 deaths worldwide, but primarily concentrated in resource-limited settings. Infections are usually spread by contaminated food and water supplies.[2−4]

Enteric fever is treated with antibiotics such as ciprofloxacin and ofloxacin.[5] However, it is difficult to diagnose clinically as it presents with nonspecific symptoms such as diarrhea, nausea and abdominal pain.[4,6] Blood and stool cultures are considered standard practice but take days to confirm a diagnosis.[7] When left untreated, enteric fever can lead to ulceration, bleeding and even multiorgan failure.[1,8] So, the speed of diagnosis is critical in achieving good outcomes following infection.

Nucleic acid tests (NATs) such as polymerase chain reactions (PCRs) provide high sensitivity, specificity and quick (1−2 h) diagnosis. However, these tests are difficult to implement in low- and middle-income countries because of the cost of laboratory facilities and trained personnel.[1,9] A frequently implemented alternative is the Widal test, a low-cost agglutination test that detects the presence of antibodies produced in response to enteric fever pathogens. Their sensitivity is generally reported around 80%, while specificity varies but is consistently reported below 50% due to cross-reacting antibodies from other enterobacteria, among other reasons.[10−12] It is, therefore, not surprising that these values are far from what is accepted by the Foundation for Innovative New Diagnostics' (FIND) enteric fever target product profiles (TPP).[13] More modern antibody-based assays, such as Typhidot and TUBEX, have similar issues with only some improvement in sensitivity and specificity.[14] An ideal test would match the performance of NATs without the need for expensive equipment or trained personnel to perform them as outlined by the REASSURED diagnostics criteria.[15]

A promising approach is CRISPR-based NATs. These assays center around a Cas12a enzyme, which is capable of binding to a guide RNA (gRNA) sequence. The gRNA has a hairpin region that binds to the Cas12a enzyme and a spacer region that can be designed to be complementary to the pathogen DNA of interest. Once the Cas12a, gRNA and target DNA form a complex, the enzyme changes conformation to reveal a nuclease domain which indiscriminately cleaves single-stranded

Received: August 5, 2024
Revised: November 30, 2024
Accepted: January 23, 2025
Published: February 6, 2025

Scheme 1. Mechanism of CRISPR-Cas12a, and The Signal Output Produced by Enzyme Trans-Cleavage and the Release of LacZ[a]

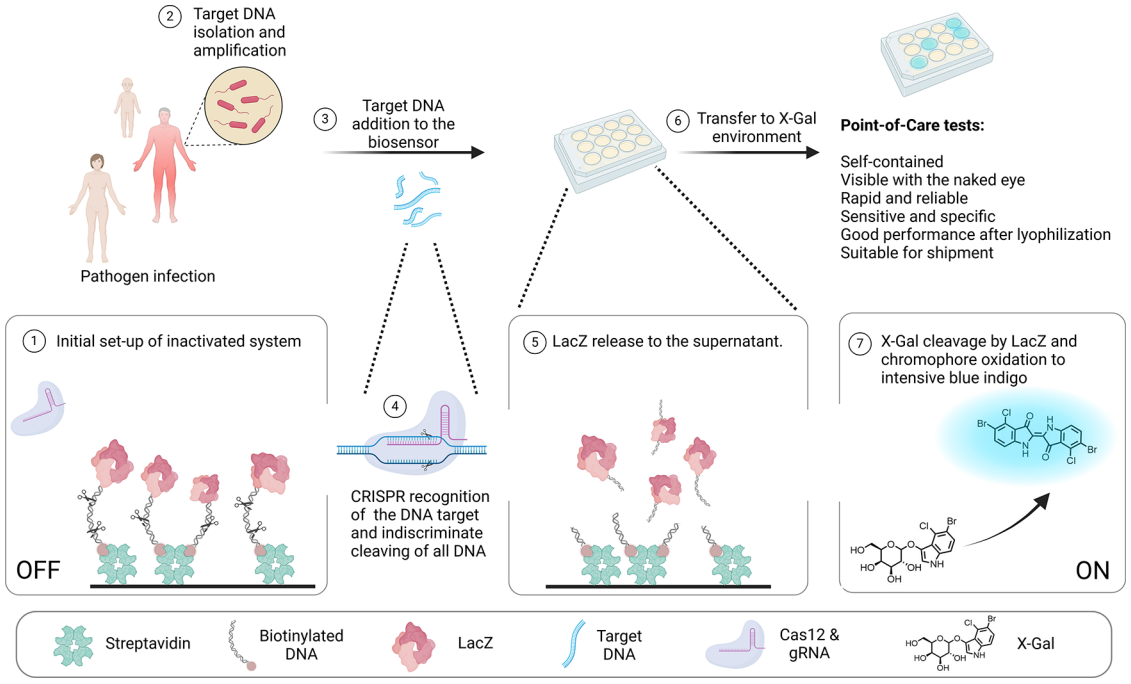

[a](1) Initial set-up of inactivated system. (2) Target DNA isolation and amplification. (3) Target DNA addition to the biosensor. (4) CRISPR recognition of the DNA target and indiscriminate cleavage of DNA. (5) LacZ release to the supernatant. (6) Transfer to an X-Gal environment. (7) X-Gal cleavage by LacZ and chromophore oxidation to intensive blue indigo [illustration created with BioRender.com].

DNA (ssDNA). This indiscriminate cleavage is known as trans-cleavage. By adding in reporters made from ssDNA with a fluorophore on one end and quencher on the other, the indiscriminate cleavage activity results in a fluorescent signal that increases proportionally with Cas12a activity. For low resource settings, one drawback of this reaction is the requirement for specialized equipment to analyze fluorescent readouts.[16]

Colorimetric readouts visible to the naked eye are preferable due to their ease of use and accessibility. Several have been reported in the last five years. A popular method in literature uses CRISPR-Cas12a reactions to control the aggregation of gold nanoparticles (AuNPs) by using ssDNA to link them together. A color change from purple to red is observed when Cas12a cleavage allows individual AuNPs to separate from each other.[17] One problem with this is that the color transitions in many existing assays are subtle and challenging to distinguish reliably with the naked eye, making it difficult for use at POC. Furthermore, AuNPs are prone to aggregation in the presence of biofluids. This can result in false negatives as aggregated nanoparticles will mimic uncleaved ssDNA.[18]

A handful of other approaches have been documented. However, only a minority use colorimetric enzymes and develop a clear color change. A description of these approaches can be found in Table S1. A benefit of using these enzymes is amplification, as each enzyme can sequentially cleave multiple substrate molecules and improve the limit of detection. These approaches immobilize the enzymes urease[19] and HRP[20,21] on a surface with an oligonucleotide. The proteins are released by CRISPR trans-cleavage activity of activated Cas12a. Then, they are transferred to an environment containing their corresponding chromogenic substrates: urea/phenol red and TMB/H_2O_2 producing clear color changes. Inspired by these assays and the scarcity of enzyme-based colorimetric assays, we aimed to develop a system with a clear colorless-to-color reaction, suitable for local manufacturing using a colorimetric enzyme produced in *E. coli*. Additionally, we sought to explore the impact of conjugate DNA length on signal and ensure the system's compatibility with ambient temperature storage.

In this paper, we propose a detection system using the highly stable LacZ enzyme. Immobilized on a surface with ssDNAs, LacZ is released and mixed with X-Gal, a β-galactosidase-cleavable substrate (Scheme 1). The released chromophore spontaneously dimerizes and oxidizes into 5,5′-dibromo-4,4′-dichloro-indigo, producing a colorimetric clear-to-blue output that is visible to the naked eye. We achieve a lower limit of detection (picomolar) than the fluorophore-quencher strategy first employed by Chen et al.,[16] explore and give insight into the difference made by the oligo linker length[22,23] and show that our assay can be lyophilized. Overall, this tool would improve the diagnosis of enteric fever in the Global South by providing an affordable solution which does not require detection equipment.

MATERIALS AND METHODS

β-galactosidase Expression and Purification. The β-galactosidase expression plasmid was produced by cloning a β-galactosidase sequence into the Addgene plasmid # 72935 (final sequence available via Zenodo 10.5281/zenodo.14693399), which was then transformed into BL21 DE3 cells (NEB). Individual colonies were picked and grown in luria broth (LB) containing 50 μg/mL carbenicillin (Melford) at 37 °C. After 16 h, the liquid culture was diluted 1:50 into 350 mL of LB-carbenicillin broth and incubated at 37 °C with shaking at 225 rpm until the OD_{600} was 0.4−0.6. At this point, the culture was induced with 1 mM isopropyl β-D-1-thiogalactopyranoside (IPTG) and incubated at 16 °C overnight at 225 rpm. The next day, cells were harvested by centrifugation at 3220*g* for 20 min and

https://doi.org/10.1021/acssensors.4c02029
ACS Sens. 2025, 10, 717−724

the pellets were resuspended in 1x PBS and 0.01 mg/mL lysozyme for lysis. The suspended cell mixture was sonicated at 15 amplitude microns for 10 cycles of 30 s on and 10 s off with a MSE Soniprep 150 Plus Ultrasonic Disintegrator (Medical and Scientific Equipment) and clarified by centrifuging at 10,000*g* for 15 min. The supernatants were filtered with a 0.2 μm filter.

The protein was purified through Ni-NTA purification using Ni-IMAC resin (Novagen, #70666-3). The following protocol was adapted from the Novagen His-Bind protocol. After running binding buffer [0.5 M NaCl, 40 mM Tris-HCl, 5 mM imidazole, pH 7.9] through the column and loading the sample, the column was washed with 10-bed volumes of binding buffer followed by 6-bed volumes of wash buffer [0.5 M NaCl, 120 mM imidazole, 40 mM Tris-HCl, pH 7.9]. The protein was finally eluted after applying 6-bed volumes of elution buffer [1 M imidazole, 0.5 M NaCl, 20 mM Tris-HCl, pH 7.9]. The final sample was buffer exchanged into 1× PBS using a CentriPure P25 column (EMP Biotech, CP-0504). The enzyme was concentrated by centrifuging it at 3200*g* for 15 min in a Pierce Protein Concentrator PES 10K MWCO (Thermo Fisher Scientific). The expression and purification results were analyzed by SDS-PAGE and 25% glycerol was added for storage at −20 °C. Protein concentrations were obtained using a NanoDrop One/OneC Microvolume UV−vis Spectrophotometer (Thermo Scientific).

Conjugation Reaction. DNA oligos with a 5′ amino modifier C12 and a 3′ biotin modification were purchased from IDT containing 20, 40, or 100 nucleotides (nt). Sequences were chosen so that secondary structures would be minimal using the NUPACK software. The 20 nt oligo was also purchased without the biotin modification (Table S2). All were mixed with 50× excess of Sulfo-SMCC dissolved in DMSO (Thermo Fisher). The final reaction contained 20% DMSO and 80% 10× PBS at pH 8.4 and was incubated at 27 °C with shaking (∼700 rpm) overnight. The sample was then dialyzed for 5 h in 10× PBS pH 8.4 buffer with a 2 kDa membrane (Fisher Scientific, #15310692) and quantified with a NanoDrop. Oligo-conjugates were characterized by HPLC and mass spectrometry. Next, 25 nmol of DNA-SMCC were mixed with 5 nmol of purified LacZ. The reaction was incubated overnight at 27 °C and 700 rpm in 3x PBS resulting from the mixing. Dialysis of the sample was carried out in 1× PBS at pH 7 with a 13 kDa (SLS, #TUB2002) or 50 kDa (Sigma, #PURX50005) membrane, depending on the DNA length, for at least 6 h.

HPLC. To characterize the oligo-protein reactions, an Agilent 1260 Infinity II was used with a Poroshell 120 EC-C18 2.7 μm 4.6 × 100 mm (Agilent) stationary phase and a mobile phase containing two buffers: buffer A [20 mM ammonium acetate at pH 7.7], and buffer B [70% buffer A and 30% acetonitrile].

For the DNA and DNA-SMCC samples, the protocol ran with 1.3 mL/min flow starting with buffer A at 100%, then a ramp from 0 to 12 min leading to 100% buffer B and finalized with another ramp from 12 to 15 min back to 100% buffer A.

gRNA Design, in vitro Transcription (IVT) and Quantification. During an in-house gRNA screening, spacer regions were selected following a TTTN protospacer adjacent motifs (PAM) sequence. Double-stranded cDNA template was annealed for gRNA transcription (Table S3). The double-stranded products were mixed with the HiScribe T7 High Yield RNA Synthesis kit (NEB) and incubated at 37 °C overnight. The gRNA product was purified using DNaseI digestion and a Monarch RNA Cleanup kit following the manufacturer's instructions (NEB). The gRNA was further quantified by NanoDrop.

Immobilization of the Conjugates on Streptavidin Plates. 384-well Clear Pierce Streptavidin Coated High-Capacity plates (Thermo Fisher) were washed 3 times with 100 μL of 1× CutsmartT buffer adapted from the NEB Cutsmart recipe [50 mM Potassium Acetate, 20 mM Tris-acetate, 10 mM Magnesium Acetate, 100 μg/mL BSA, 0.1% tween-20, pH 7.9]. All conjugates were diluted in the same buffer so that 1 pmol of enzyme monomer was added in 50 μL of buffer unless the concentration was otherwise specified. The conjugate was incubated for 2 h at room temperature with shaking. After this time, the conjugate solution was removed, and the wells were washed 3 times with 1× CutsmartT. 35 μL of 5 mg/mL X-Gal were added with final buffer contents being 80% 1× PBS, 10% DMF and 10% DMSO to confirm that the conjugates were attached to the plates. The absorbance at 600 nm was collected at 37 °C using a BMG Labtech plate reader. For 96-well streptavidin plates, all volumes were doubled but concentrations remained the same.

CRISPR Trans-cleavage of Immobilized Conjugates. The protocol above was followed for binding up until the second washing step. At this point, 35 μL of CRISPR reaction in 1× CutsmartT were added containing 75 nM LbaCas12a (NEB), 95 nM gRNA and varying concentrations of 60 bp synthetic dsDNA target. Negative controls included reactions without the synthetic target or without the target and gRNA. Benzonase (Sigma) was used as a positive control in the same buffer at 1 unit concentration. The reactions were incubated for 1 h at 37 °C and the 35 μL of solutions were transferred to a 384-well clear plate (Greiner). 35 μL of 5 mg/mL X-Gal, as previously described, were added to the cleavage solution. The absorbance at 600 nm was read at 37 °C using a BMG Labtech plate reader for 45 min.

The CRISPR reaction added in this assay was also tested separately with 1, 0.5, and 0.1 μM of 5′ 6-FAM (Fluorescein)-TTATT- 3′ Iowa Black (FQ) reporter (IDT) and the fluorescence (480 excitation, 520 emission) was measured at 37 °C.

The colorimetric reaction was also tested with PCR amplicons of extracted Typhi DNA (Table S4) and 60 bp synthetic dsDNA off-targets all of which contained a PAM sequence (Table S5).

Limit of Detection Data Analysis. All absorbance graphs were normalized by averaging the absorbance at 600 nm of the replicates in each condition at 45 min and subtracting the average value at 0 min. To obtain the % signal in the limit of detection assays, that value was divided by the maximum signal across all conditions and multiplied by 100. These values were plotted against the log10 of the target concentrations used. The slopes of the points before and after signal increase were obtained and the intersection of the two calculated resulting in the limit of detection for each condition.

Typhi Culture, Extraction and Amplification. *Salmonella* Typhi BRD948 (Ty2 ΔaroC ΔaroD ΔhtrA) was grown in 0.2 μm filtered 0.4 mg/mL phenylalanine (Sigma), 0.4 mg/mL tryptophan (Sigma), 0.1 mg/mL para-aminobenzoic acid (Sigma), 0.1 mg/mL dihydro-oxbenzoic acid (Thermo Fisher) and 0.4 mg/mL tyrosine (sodium salt) (Sigma) 10 mL LB solution overnight shaken at 200 rpm at 37 °C in a 50 mL conical tube. Genomic DNA was extracted using a Monarch Genomic DNA Purification Kit and quantified using a Nanodrop as above.

Lyophilization. Conjugates were bound, washed, and the CRISPR reaction mixed and added, as above, the only exceptions being that no targets were added, and any Cas dilutions were made into buffers lacking glycerol. The final reactions also contained 10% trehalose dihydrate. The wells were covered in parafilm with a hole above each well and frozen at −80 °C. After 1 h, the plate was introduced in a VirTis Advantage lyophilizer and the following protocol was run: −45 °C for 3 h, −5 °C for 2 h and 20 °C for 1 h with a ramp of 0.1 °C/min. The vacuum was held constant at 50 mTorr. After lyophilization, the reactions were rehydrated with and without the target at 7.5 nM and incubated for an hour at 37 °C before the addition of X-Gal to the supernatant.

RESULTS AND DISCUSSION

Conjugate Synthesis. Optimization of pH and salt concentration to obtain DNA-*N*-Hydroxysuccinimide (NHS) conjugates was undertaken using aminylated 20 nt DNA without biotin (DNA_{20}) and fluorescein-NHS (Thermo Fisher). Within the tested range of PBS concentrations (1× to 10×), higher concentrations gave higher reaction yields. Yields were calculated by dividing the fluorescence by the DNA concentration. The effect of volume was also tested but showed no difference (Figure S1). Reactions were unsuccessful at pH 7 in all conditions tested but did work at pH 8.4.

https://doi.org/10.1021/acssensors.4c02029
ACS Sens. 2025, 10, 717−724

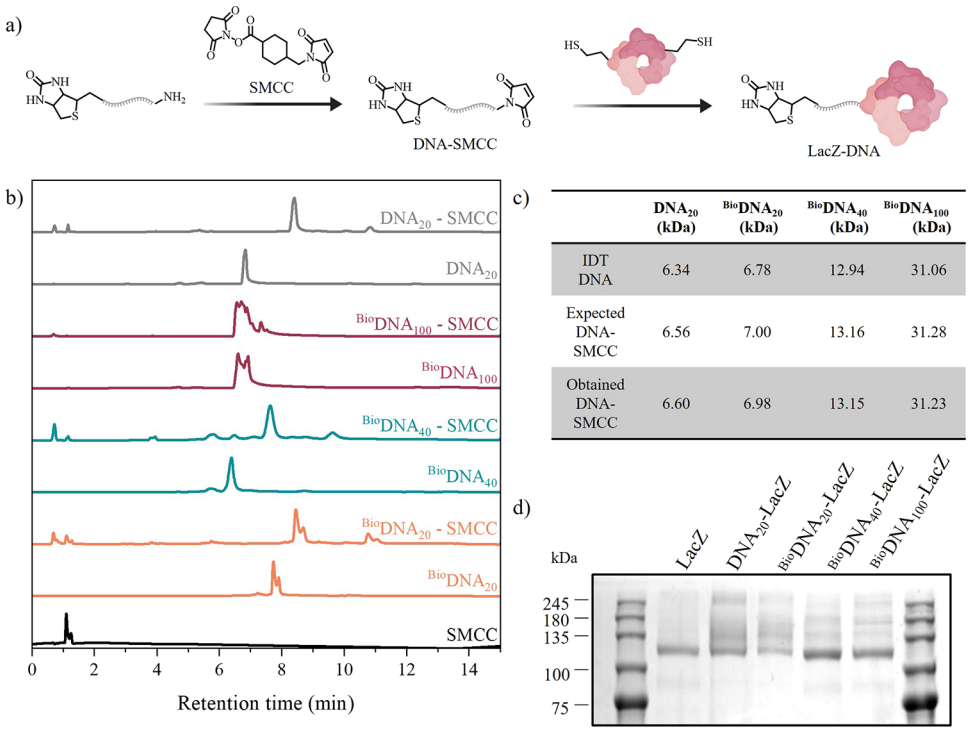

	DNA_{20} (kDa)	$^{Bio}DNA_{20}$ (kDa)	$^{Bio}DNA_{40}$ (kDa)	$^{Bio}DNA_{100}$ (kDa)
IDT DNA	6.34	6.78	12.94	31.06
Expected DNA-SMCC	6.56	7.00	13.16	31.28
Obtained DNA-SMCC	6.60	6.98	13.15	31.23

Figure 1. Conjugate characterization. (a) Schematic of the conjugation reaction between the aminylated DNA, the SMCC linker and LacZ [illustration created with ChemDraw and BioRender.com]. (b) HPLC data of the SMCC linker, aminylated oligos of all lengths and the conjugation of the oligos with the linker. (c) Mass spectrometry values of the modified DNA before and after conjugation. (d) SDS-PAGE of LacZ at ∼118 kDa vs DNA-LacZ conjugates at the same and higher masses. The full SDS-PAGE image can be found in Figure S3.

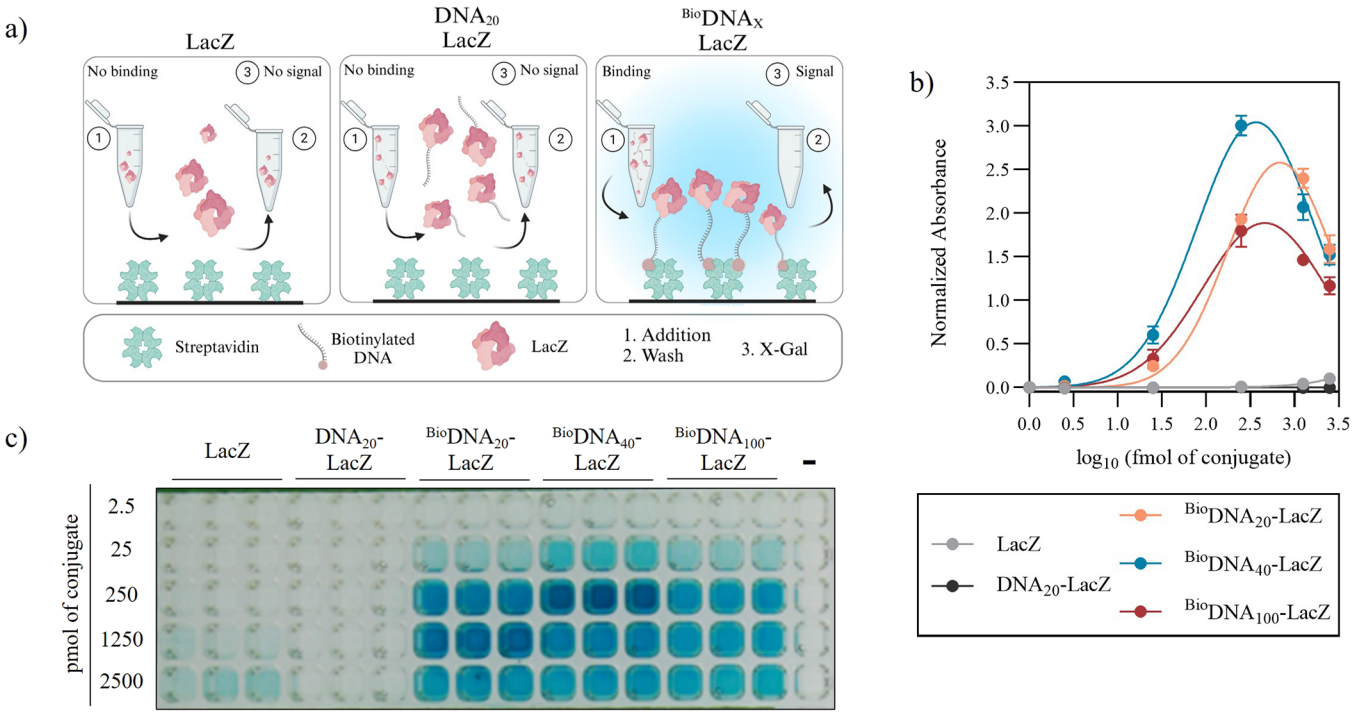

Figure 2. Conjugates Binding Titration. (a) Schematic of the two experimental controls which lack biotin, or DNA and biotin, as well as the full conjugates, and the expected colorimetric outcome after binding to streptavidin [illustration created with BioRender.com]. (b) Absorbance graph of a titration of conjugates with various lengths of DNA (N = 3). (c) Photograph of assay results after 45 min of incubation (n = 3).

Once the reaction was optimized, 20, 40, and 100 nt long aminylated (5′) and biotinylated (3′) ssDNAs were reacted with a cross-linker containing an NHS ester (Figure 1a). The resulting reaction was characterized via HPLC. Compared to unconjugated DNA, the reaction had a higher retention time in the column producing a peak shift for all conjugates. Using a C18 column, which separates molecules by polarity, we hypothesize that the more similar retention times of DNA_{100}

https://doi.org/10.1021/acssensors.4c02029
ACS Sens. 2025, 10, 717−724

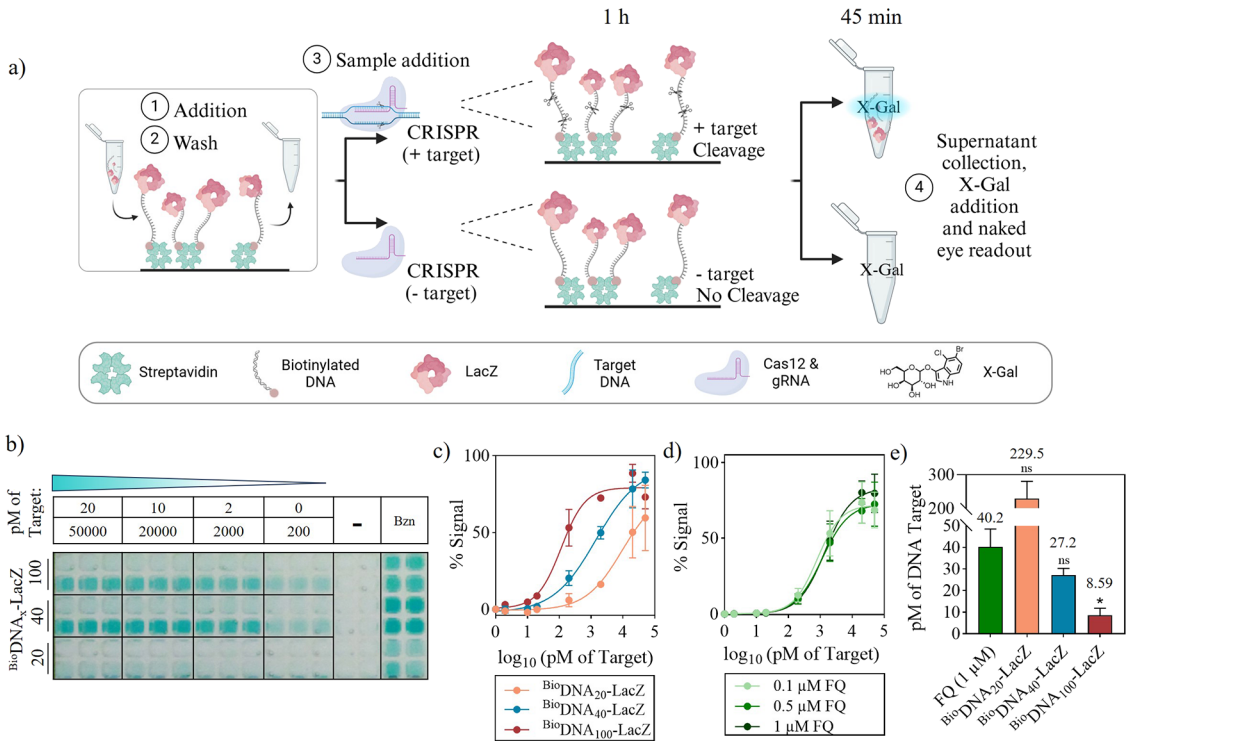

Figure 3. Limit of detection of the CRISPR assay. (a) Schematic of the CRISPR assay in the presence of DNA-LacZ conjugates [illustration created with BioRender.com]. (b) Photograph of the transferred supernatant following the CRISPR limit of detection assay and incubation with X-Gal for 45 min ($n = 3$). (c) % Signal from absorbance values of the three conjugates LoD assay in part (b) ($N = 3$). (d) % Signal from fluorescence values of the CRISPR limit of detection assay using fluorescent probes at varying concentrations ($N = 3$). (e) Calculated limits of detection of each conjugate compared to the fluorescent probe. Asterisks represent significance compared to the FQ control where $P < 0.05$.

peaks with and without linker result from the negligible hydrophobicity change caused by the linker's small size relative to the 100 nt DNA (Figure 1b). MALDI-TOF was performed to verify the molecular weight of the reacted species (Figures 1c). In some cases, we observed a slightly different expected mass which is likely due to the ionization process (more details in Figure S2).

Oligonucleotides covalently bound to the cross-linker were incubated in the presence of LacZ to couple the accessible thiols on the enzyme with the reactive maleimide on the linker. After purification, the resulting conjugates were verified by SDS-PAGE which showed bands with higher molecular weights compared to the original LacZ enzyme indicating one or more covalent modifications with the DNA (Figures 1d and S3). The reaction yields were estimated by calculating the enzyme concentration using a LacZ activity standard curve and calculating the ssDNA concentration using a Qubit device.

Conjugate Binding Titration. In order to optimize the conjugate immobilization, the DNA-LacZ conjugates produced were incubated in streptavidin-coated plates at varying concentrations and washed before the addition of X-Gal (Figure 2a). Negative control samples were utilized: unconjugated LacZ and a 20 nt conjugate without biotin (DNA_{20}-LacZ). These samples showed minimal binding to the plate, with a slight color development at the highest concentrations, though this had overall negligible impact. In contrast, the three biotinylated conjugates remained active while bound producing a visible blue color upon addition of X-Gal. The color intensity did not always increase with the concentration of conjugate added, however. We found an optimal concentration between 250 and 1250 fmol of conjugate (Figure 2b,c). It is likely that the higher concentration used inhibits diffusion and reduces binding. Given that the plate manufacturer indicates the binding capacity to be around 60 pmol D-biotin/well, we speculate that the size of LacZ (472 kDa) may be causing steric hindrance, reducing the space available for molecules to bind to streptavidin (60 kDa).

CRISPR conjugate cleavage limit of detection. To colorimetrically detect a *S.* Typhi DNA sequence, we exploited the trans-cleavage property of CRISPR-Cas12a. In the presence of the gRNA/target hybrid, this property was activated and Cas12a cleaved the biotinylated-LacZ hybrid from the streptavidin surface. This produced an intense blue color after transferring the supernatant to a plate containing X-Gal. This was replicated with benzonase in place of Cas12a, acting as a positive control for nuclease activity. In the absence of this target and/or gRNA, the blue color either did not appear or was faint after 45 min of incubation (Figure 3a). This time was chosen because background starts to be observed afterward. Waiting until the reaction plateaued was not feasible due to the hydrolysis product of X-Gal precipitating at high concentrations. Kinetic details can be found in Figure S4.

A limit of detection study was performed by adding various target concentrations of *S.* Typhi synthetic DNA during the CRISPR reaction step (50 nM, 20 nM, 2 nM, 200 pM, 20 pM, 2 pM and 0 pM). After 45 min of supernatant incubation with X-Gal, we found limits of detection were inversely proportional to the length of DNA on the conjugate: 229.5, 27.2, and 8.59 pM from the shortest to the longest conjugate. The LoDs after 15-, 25- and 35 min incubation were similar (Figure S5). The

https://doi.org/10.1021/acssensors.4c02029
ACS Sens. 2025, 10, 717−724

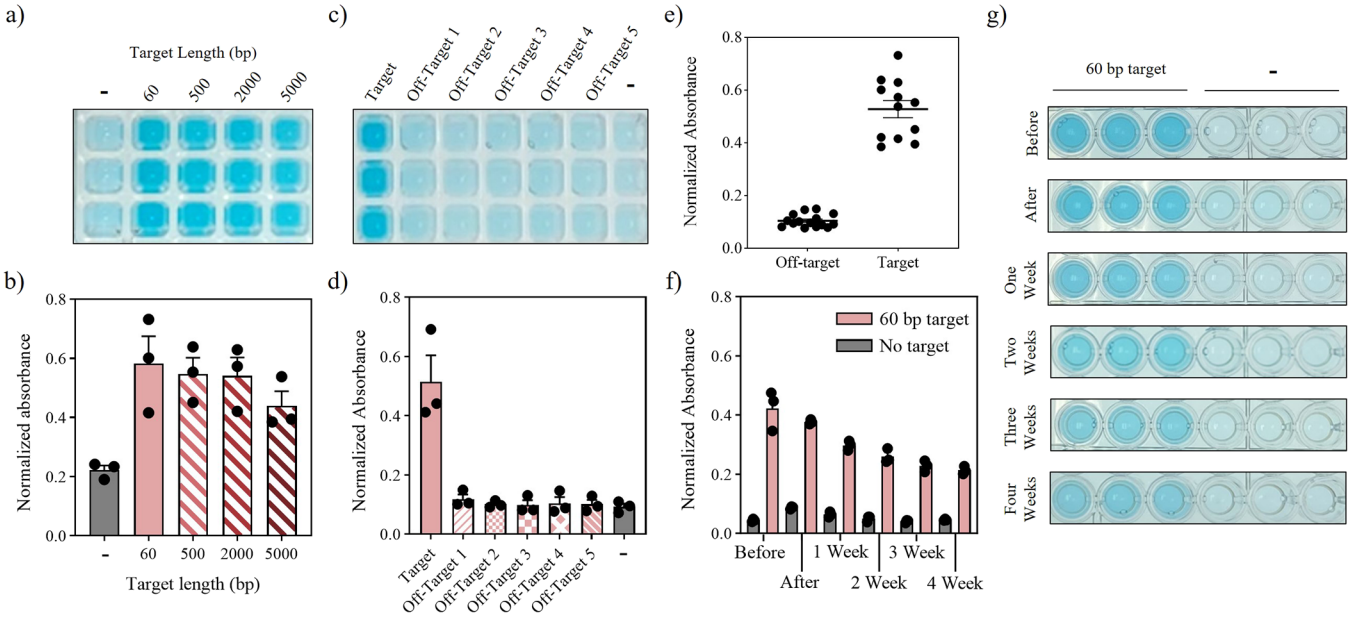

Figure 4. Conjugate cleavage with various targets and lyophilization. (a) Image of one replicate of figure (b) after a 45 min incubation. (b) Normalized absorbance after CRISPR cleavage activation with various *S.* Typhi amplicons ($N = 3$). (c) Photograph of one replicate of figure (d) after a 45 min incubation. (d) Normalized absorbance after CRISPR cleavage activation with the addition of various off-target sequences ($N = 3$). (e) Average values of normalized absorbance after CRISPR cleavage with and without the correct target sequence. (f) Normalized absorbance of CRISPR cleavage activation immediately before, after and weeks after lyophilization ($N = 3$). (g) Photographs of part (f) after a 45 min incubation.

limit of detection was also analyzed visually which increased to 200 pM for the 40 and 100 nt conjugates, and 20 nM for the 20 nt conjugate (Figure 3b,c). From these results it could be hypothesized that longer DNA would produce a lower limit of detection allowing more room for Cas12a to reach the DNA between the bottom of the well and LacZ. However, the synthesis cost would increase significantly above 100 nt. Our benchmark CRISPR diagnostic assay used a standard fluorescent reporter that had a LoD of 40.2 pM which is comparable to the 20 and 40 nt conjugates but is significantly higher than the LoD of the 100 nt conjugate of 8.59 pM (Figure 3d,e). P-values for the *t* test performed between LoDs can be found in Supplementary Table S6. Our system thus delivers the benefit of colorimetric readout with higher sensitivity compared to fluorescence, which is typically more sensitive due to lower background noise.

Conjugate Cleavage with Various DNA Sequences. In addition to using synthetic DNA targets, the system was tested with PCR amplified *S.* Typhi genomic DNA. The amplified targets were of various sizes: 500, 2000, and 5000 bp (Figure S6). The change in absorbance obtained for all targets was similar to a decreasing trend as DNA length increased but still a clear color difference at 5000 bp compared with the negative control (Figure 4a,b). This flexibility suggests that this system could be paired with a range of amplification techniques such as RPA and LAMP, which produce amplicons under 1000 bp.[24,25] Direct detection of genomic DNA could pose challenges, but emerging techniques such as genomic shearing[26] and cascade amplifications[27] are improving enzyme sensitivity. To investigate sequence specificity of the gRNAs, the system was tested further using short synthetic dsDNA strands that contained identical PAM sequences but with spacer regions that differed from the target. All off-target sequences performed very similarly to the no target reactions (Figure 4c,d). Combining all data for target amplicons and off-target samples (Figure 4e), a receiver operating characteristic (ROC) curve shows that the system discriminated well between reactions with and without the correct target sequence with an area under the curve of 1.00 (Figure S7).

Lyophilization. In most laboratories or clinics, protein-based diagnostics are stored in a fridge or freezer to maintain activity. A cold chain would be necessary during the shipping process which would increase costs. Lyophilization (or freeze-drying) would eliminate the need for a cold chain and allow for storage of the diagnostic at room temperature. We tested several lyophilization formulations with the aim of maintaining the structural integrity of LacZ and Cas12a together during lyophilization. Most of the additives tested successfully preserved LacZ activity, while trehalose dihydrate proved to be the most effective in retaining Cas12a activity. As a result, trehalose dihydrate was selected to be included prior to the lyophilization of our system. Further details can be found in Figure S8.

In our system, the immobilized conjugates were freeze-dried in the presence of Cas12a and a gRNA. After lyophilization, the reactions were rehydrated with and without the target and the absorbance measured. The reactions were also tested before lyophilization in the same conditions to account for the inhibitory effect of trehalose dihydrate. Even in the presence of the sugar, there was a clear color distinction between the samples with target and without. When comparing the activity of the samples before and after lyophilization, there was little difference between the two indicating that the enzymes maintained their folded structure and activity. The activity of the system was also tested every week for 4 weeks after lyophilization and storage at room temperature. While absorbance decreased over time, a clear blue color was observed in the samples with target compared to those without throughout the stability assay. The difference was deemed significant through statistical analysis (Table S7) and was obvious when visualized with the naked eye (Figure 4f,g).

https://doi.org/10.1021/acssensors.4c02029
ACS Sens. 2025, 10, 717−724

CONCLUSIONS

This study developed a colorimetric CRISPR system clearly visible to the naked eye with a comparable limit of detection to the gold-standard FQ visualization system. The assay was successful in the presence of *S.* Typhi amplicons, as well as synthetic DNA, with a limit of detection of 8.59 pM, and remained colorless if the target DNA sequence was not present. To extend previous similar work, the length of the immobilizing oligos was varied, and the absorbance produced was directly proportional to length. The combined assay with the CRISPR and colorimetric reactions occurred in less than 2 h, which is amenable to a POC setting. Lyophilization of the system was successful for 4 weeks, so we anticipate that shipping will be possible without cold chain. In future work, optimization would involve coupling the Cas12a detection with an easy amplification technique to reach higher levels of sensitivity, applying the assay to clinical samples, and developing integrated diagnostic devices where the sample preparation, diagnostic assay and readout can be performed sequentially. It will also be important to modify this two-step assay to have a one-pot reaction, further simplifying its use. To achieve this, we are exploring enzyme modifications that render the immobilized LacZ enzyme inactive, or that enable inducible activation of the reaction following cleavage. In addition to detecting *S.* Typhi, our approach would be readily applicable to detection of other nucleic acid targets, and as a readout module for any CRISPR/Cas trans-cleavage based assay.

ASSOCIATED CONTENT

Data Availability Statement

All data supporting the findings of this study are available within the paper and its Supporting Information or are openly available in Zenodo at 10.5281/zenodo.14693399

Supporting Information

The Supporting Information is available free of charge at https://pubs.acs.org/doi/10.1021/acssensors.4c02029.

Table of published colorimetric assays, sequences for all nucleic acids, additional experimental results, and statistical analysis (PDF)

AUTHOR INFORMATION

Corresponding Author

Jennifer C. Molloy − *Department of Chemical Engineering and Biotechnology, University of Cambridge, Cambridge CB3 0AS, United Kingdom;* orcid.org/0000-0003-3477-8462; Email: jcm80@cam.ac.uk

Authors

Ana Pascual-Garrigos − *Department of Chemical Engineering and Biotechnology, University of Cambridge, Cambridge CB3 0AS, United Kingdom*

Beatriz Lozano-Torres − *Department of Chemical Engineering and Biotechnology, University of Cambridge, Cambridge CB3 0AS, United Kingdom*

Akashaditya Das − *Department of Chemical Engineering, Imperial College London, London SW7 2AZ, United Kingdom*

Complete contact information is available at: https://pubs.acs.org/10.1021/acssensors.4c02029

Author Contributions

A.P.-G.: conceptualization, methodology, investigation, validation, writing - original draft and visualization. B.L.-T.: methodology, investigation, writing - review and editing and supervision. A.D.: conceptualization, writing - review and editing. J.C.M.: conceptualization, supervision, writing - review and editing and funding acquisition.

Funding

Trinity College External Research Studentship to APG; Trinity College Paterson Fund to A.P.-G; MSCA-UKRI guarantee Fellowship to B.L.-T; Shuttleworth Foundation Fellowship to J.C.M.; University of Cambridge EPSRC GCRF Impact Acceleration Account to J.C.M.

Notes

The authors declare no competing financial interest.

ACKNOWLEDGMENTS

This research was supported by the mass spectrometry team in the Department of Chemistry at the University of Cambridge. Dr. Derek Pickard (JCBC, Addenbrookes site) provided the *S.* Typhi genomic DNA. We also thank Dr. Steve Baker and Dr. Jim Ajioka for helpful feedback and discussion.

ABBREVIATIONS

Cas12a, CRISPR-associated protein 12a; CRISPR, clustered regularly interspaced short palindromic repeats; dsDNA, double-stranded DNA; FQ, fluorophore-quencher ssDNA; gRNA, guide RNA; HRP, horseradish peroxidase; HPLC, high-performance liquid chromatography; IVT, in vitro transcription; LacZ, β-galactosidase; LB, luria broth; MALDI-TOF, matrix assisted laser desorption ionization-time-of-flight mass spectrometry; NAT, nucleic acid test; NHS, *N*-Hydroxysuccinimide; POC, point-of-care; ROC, receiver operating characteristic; ssDNA, single-stranded DNA; X-Gal, 5-Bromo-4-chloro-3-indolyl β-D-galactopyranoside

REFERENCES

(1) Bhandari, J.; Thada, P. K.; DeVos, E. Typhoid Fever. In *StatPearls*; StatPearls Publishing: Treasure Island (FL), 2022.

(2) Typhoid. https://www.who.int/news-room/fact-sheets/detail/typhoid (accessed April 01, 2024).

(3) Antillón, M.; Warren, J. L.; Crawford, F. W.; Weinberger, D. M.; Kürüm, E.; Pak, G. D.; Marks, F.; Pitzer, V. E. The Burden of Typhoid Fever in Low- and Middle-Income Countries: A Meta-Regression Approach. *PLoS Negl. Trop. Dis.* **2017**, *11* (2), No. e0005376.

(4) Neupane, D. P.; Dulal, H. P.; Song, J. Enteric Fever Diagnosis: Current Challenges and Future Directions. *Pathogens* **2021**, *10* (4), 410.

(5) Effa, E. E.; Lassi, Z. S.; Critchley, J. A.; Garner, P.; Sinclair, D.; Olliaro, P. L.; Bhutta, Z. A. Fluoroquinolones for Treating Typhoid and Paratyphoid Fever (Enteric Fever). *Cochrane Database Syst. Rev.* **2019**, *2019* (10), No. CD004530.

(6) Mogasale, V.; Ramani, E.; Mogasale, V. V.; Park, J. What Proportion of Salmonella Typhi Cases Are Detected by Blood Culture? A Systematic Literature Review. *Ann. Clin. Microbiol. Antimicrob.* **2016**, *15*, 32.

(7) Marchello, C. S.; Birkhold, M.; Crump, J. A. Complications and Mortality of Typhoid Fever: A Global Systematic Review and Meta-Analysis. *J. Infect.* **2020**, *81* (6), 902−910.

(8) Saha, T.; Arisoyin, A. E.; Bollu, B.; Ashok, T.; Babu, A.; Issani, A.; Jhaveri, S.; Avanthika, C. Enteric Fever: Diagnostic Challenges and the Importance of Early Intervention. *Cureus* **2023**, *15* (7), No. e41831.

(9) Baker, S.; Favorov, M.; Dougan, G. Searching for the Elusive Typhoid Diagnostic. *BMC Infect. Dis.* **2010**, *10*, 45.

(10) Mawazo, A.; Bwire, G. M.; Matee, M. I. N. Performance of Widal Test and Stool Culture in the Diagnosis of Typhoid Fever among Suspected Patients in Dar Es Salaam, Tanzania. *BMC Res. Notes* **2019**, *12* (1), 316.
(11) Deksissa, T.; Gebremedhin, E. Z. A Cross-Sectional Study of Enteric Fever among Febrile Patients at Ambo Hospital: Prevalence, Risk Factors, Comparison of Widal Test and Stool Culture and Antimicrobials Susceptibility Pattern of Isolates. *BMC Infect. Dis.* **2019**, *19* (1), 288.
(12) Saeed, E. A.; Singh, S.; Trivedi, S. Study of various laboratory methods for an early diagnosis of enteric fever *Journal of Molecular Imaging & Dynamics*, 2021.
(13) Mather, R. G.; Hopkins, H.; Parry, C. M.; Dittrich, S. Redefining Typhoid Diagnosis: What Would an Improved Test Need to Look Like? *BMJ. Glob. Health* **2019**, *4* (5), No. e001831.
(14) Wijedoru, L.; Mallett, S.; Parry, C. M. Rapid Diagnostic Tests for Typhoid and Paratyphoid (Enteric) Fever. *Cochrane Database Syst. Rev.* **2017**, *2017* (5), No. CD008892.
(15) Land, K. J.; Boeras, D. I.; Chen, X.-S.; Ramsay, A. R.; Peeling, R. W. REASSURED Diagnostics to Inform Disease Control Strategies, Strengthen Health Systems and Improve Patient Outcomes. *Nat. Microbiol.* **2019**, *4* (1), 46−54.
(16) Chen, J. S.; Ma, E.; Harrington, L. B.; Costa, M. D.; Tian, X.; Palefsky, J. M.; Doudna, J. A. CRISPR-Cas12a Target Binding Unleashes Indiscriminate Single-Stranded DNase Activity. *Science* **2018**, *360*, 436 DOI: 10.1126/science.aar6245.
(17) Zhang, W. S.; Pan, J.; Li, F.; Zhu, M.; Xu, M.; Zhu, H.; Yu, Y.; Su, G. Reverse Transcription Recombinase Polymerase Amplification Coupled with CRISPR-Cas12a for Facile and Highly Sensitive Colorimetric SARS-CoV-2 Detection. *Anal. Chem.* **2021**, *93* (8), 4126−4133.
(18) Leopold, L. F.; Tódor, I. S.; Diaconeasa, Z.; Rugină, D.; Ştefancu, A.; Leopold, N.; Coman, C. Assessment of PEG and BSA-PEG Gold Nanoparticles Cellular Interaction. *Colloids Surf. Physicochem. Eng. Asp.* **2017**, *532*, 70−76.
(19) Ki, J.; Na, H.-K.; Yoon, S. W.; Le, V. P.; Lee, T. G.; Lim, E.-K. CRISPR/Cas-Assisted Colorimetric Biosensor for Point-of-Use Testing for African Swine Fever Virus. *ACS Sens.* **2022**, *7* (12), 3940−3946.
(20) Mu, X.; Li, J.; Xiao, S.; Xu, J.; Huang, Y.; Zhao, S.; Tian, J. Peroxidase-Mimicking DNA-Ag/Pt Nanoclusters Mediated Visual Biosensor for CEA Detection Based on Rolling Circle Amplification and CRISPR/Cas 12a. *Sens. Actuators B Chem.* **2023**, *375*, No. 132870.
(21) Hu, M.; Yuan, C.; Tian, T.; Wang, X.; Sun, J.; Xiong, E.; Zhou, X. Single-Step, Salt-Aging-Free, and Thiol-Free Freezing Construction of AuNP-Based Bioprobes for Advancing CRISPR-Based Diagnostics. *J. Am. Chem. Soc.* **2020**, *142* (16), 7506−7513.
(22) Ivanov, A. V.; Safenkova, I. V.; Zherdev, A. V.; Wan, Y.; Dzantiev, B. B. Comparison of Single-Stranded DNA Probes Conjugated with Magnetic Particles for Trans-Cleavage in Cas12a-Based Biosensors. *Biosensors* **2023**, *13* (7), 700.
(23) Burkin, K. M.; Ivanov, A. V.; Zherdev, A. V.; Dzantiev, B. B.; Safenkova, I. V. A Critical Study on DNA Probes Attached to Microplate for CRISPR/Cas12 Trans-Cleavage Activity. *Biosensors* **2023**, *13* (8), 824.
(24) Kellner, M. J.; Koob, J. G.; Gootenberg, J. S.; Abudayyeh, O. O.; Zhang, F. SHERLOCK: Nucleic Acid Detection with CRISPR Nucleases. *Nat. Protoc.* **2019**, *14* (10), 2986−3012.
(25) Broughton, J. P.; Deng, X.; Yu, G.; Fasching, C. L.; Servellita, V.; Singh, J.; Miao, X.; Streithorst, J. A.; Granados, A.; Sotomayor-Gonzalez, A.; Zorn, K.; Gopez, A.; Hsu, E.; Gu, W.; Miller, S.; Pan, C.-Y.; Guevara, H.; Wadford, D. A.; Chen, J. S.; Chiu, C. Y. CRISPR−Cas12-Based Detection of SARS-CoV-2. *Nat. Biotechnol.* **2020**, *38* (7), 870−874.
(26) Fragmentation of genomic DNA using Covaris g-Tubes prior to library preparation for sequencing|bioRxiv. https://www.biorxiv.org/content/10.1101/2024.05.29.596380v2. (accessed Oct 23, 2024).
(27) Zhang, H.; Yao, S.; Sheng, R.; Wang, J.; Li, H.; Fu, Y.; Li, J.; Zhang, X.; Zhao, C. A Cascade Amplification Strategy for Ultrasensitive *Salmonella Typhimurium* Detection Based on DNA Walker Coupling with CRISPR-Cas12a. *J. Colloid Interface Sci.* **2022**, *625*, 257−263.

https://doi.org/10.1021/acssensors.4c02029
ACS Sens. 2025, 10, 717−724